REPORT NO. AR-G-002
DATE 11 March 1960
NO. OF PAGES 32

CONVAIR | ASTRONAUTICS
CONVAIR DIVISION OF GENERAL DYNAMICS CORPORATION

HYPERSONIC GLIDE VEHICLE DESIGN CONSIDERATIONS

PREPARED BY W. F. Radcliffe
W. F. Radcliffe

CHECKED BY _____

APPROVED BY _____

APPROVED BY _____

REVISIONS

NO	DATE	BY	CHANGE	PAGES AFFECTED

FOREWORD

This report presents an integration of the advanced glide vehicle concepts which have developed at Convair-Astronautics in the course of their REA studies. The report is presented to stimulate discussion concerning the merits of the concepts proposed.

TABLE OF CONTENTS

1.0 INTRODUCTION

Initial investigations of hypersonic gliders centered around their use as vehicles to carry payloads over long distances by flight through the atmosphere. These vehicles were to be rocket boosted to high velocity within the atmosphere, and, by airborne flight at a lift to drag ratio of the order of six or more, intercontinental ranges may be attained. However, the pure ballistic missile has superseded this application of the hypersonic glider and interest has therefore been directed toward its use for manned return to the earth from satellite orbits.

The principle advantages of the glide vehicle over the pure drag re-entry vehicle for orbital re-entry lie in the reduced re-entry decelerations and the potential maneuverability of the glider which will permit more accurate landing. The maneuverability will in principle permit greater latitude in the conditions for the initiation of re-entry when arbitrary landing areas are specified.

While the glide vehicle possesses the foregoing operational advantages over the drag vehicle, it must be competitive in all areas. In particular, for a given useful load, the gross weight of the glide vehicle must compare favorably with the gross weight of a corresponding drag re-entry vehicle since this weight must initially be boosted into orbit. While the glide vehicle may perform a more extensive mission such as controlled landing, it is essential that the weight penalties for such sophistication be realized and evaluated in terms of their worth to the overall mission.

In order to assess their relation to each other, some comparison of the basic characteristics of these two vehicles is in order. As with the drag re-entry vehicle (NASA Mercury type) the design of the glider is largely dictated by aerodynamic heating considerations. It is found that if re-radiation from the surface is ignored, the total heat transferred to the glide vehicle exceeds that transferred to the drag vehicle because of the reduced deceleration and corresponding extended time of flight at high velocity. If this heat is to be absorbed by heat sink or mass loss where, in either case, the heat protection system is characterized by a gross coolant heat capacity in terms of Btu per pound of weight, then the glider would require more pounds of heat protection than the drag vehicle. However, it is within the design capability of the glider to achieve surface heat transfer rates low enough that the heat may be re-radiated by surface temperatures attainable with presently available structural materials.

In general, this requires the design of a low wingloading vehicle. It should be noted that similar techniques for radiation cooling can not be readily utilized with the pure drag vehicle unless enormous light weight drag surfaces are used to provide deceleration at very high altitudes. The structural design problem for the glide vehicle is therefore concerned with producing a lightweight lifting structure which compares favorably with the corresponding structure and heat protection system for the drag re-entry vehicle.

With respect to maneuverability, the pure drag vehicle is clearly quite limited. Maneuverability depends primarily on the lift to drag ratio of the vehicle. If long range gliding flight is not of major concern, then modest lift to drag ratios of 0.5 are sufficient to achieve the reductions in heat transfer rate required for the glider and supersonic lift to drag ratios between 1.5 and 2.0 will provide adequate maneuverability. Surface landing will require subsonic lift to drag ratios of approximately 3.0.

The remainder of this report will discuss detail design considerations pertinent to the development of re-entry gliders. In the following section, aerothermodynamic affects relating to such vehicles will be considered and specific configurations described. Structural aspects are then discussed and the concept of a lightweight pressurized structure is introduced. The basic elements of this structure are analysed to the point where approximate structural weight estimates can be made.

2.0 Aerothermodynamic Design

Heat transfer estimates for re-entry gliders have drawn heavily on nose cone technology. In general, this technology has utilized the Newtonian flow approximation to establish the local inviscid flow on the body and semi-empirical heat transfer data to determine the heating conditions. These approaches have been satisfactory for nose cones because they are simple geometric shapes of a rotationally symmetric nature. Glide vehicle configurations are considerably more complex from an analysis standpoint since in order to produce any lift they must be either unsymmetric or unsymmetrically oriented. Nevertheless, the direct application of the foregoing analysis techniques has been made to glide vehicle components with detailed flow features considered only to the extent of the gross effects estimated by Newtonian flow. By way of explanation, it should be noted that Newtonian flow assumes that the oncoming flow impacts directly on an inclined surface, losing all of its momentum normal to this surface in the process. This loss of momentum is converted to body surface pressure and the fluid is assumed to flow past the inclined surface with its original tangential component of velocity. The actual details of the flow such as the presence of shock waves or expansion waves is neglected. The principal justification for this type of analysis is its agreement with experiment for simple shapes.

2.1 Conical Flow

In view of the shortcomings of Newtonian flow in providing a basic insight into the flow phenomenon, it appears desirable to investigate a flow model which provides more information on the flow itself. Such a model is provided by the flow about a conical body. For this body, the oncoming flow is deflected by a conical shock attached to the cone apex. Solutions to this type of flow have been obtained for the case where the cone is aligned with the flow direction. They show that the flow properties (velocity, pressure and temperature) are constant along radial lines emanating from the apex.

If a body is considered which consists only of the lower portion of such a cone, (See Figure 1, Page 4) the body will have the shape of a delta wing with a curved lower surface. The basic features of this configuration are established by the cone angle θ_c and the meridion angle ϕ. The sweep angle λ may be calculated from the two

FIGURE 1

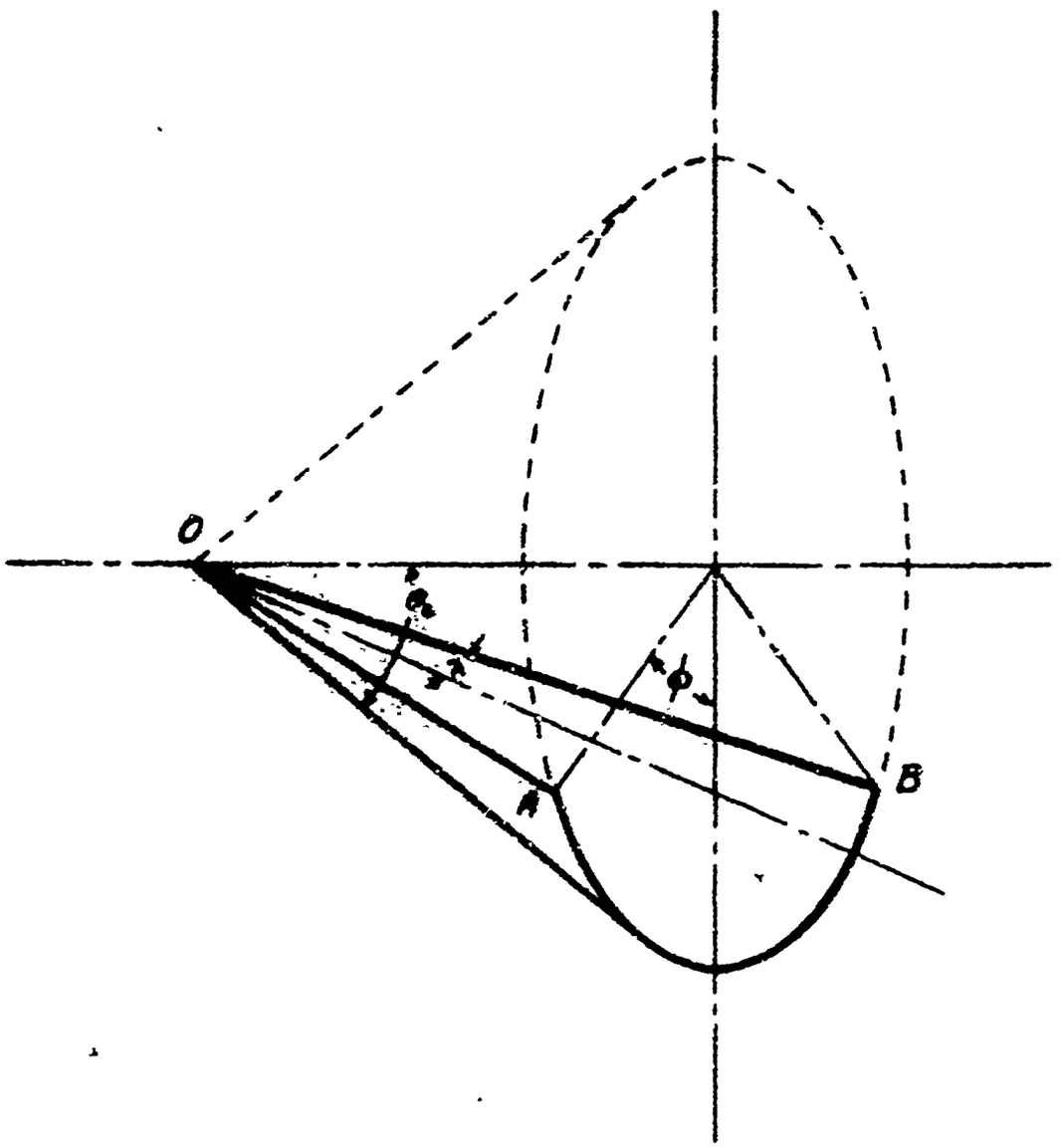

FIGURE 1

given angles θ_c and ϕ. To a first approximation, the flow about such a body will be conical and identical to the flow about a complete cone. Since low pressures will exist on the upper surface, there will be a local expansion around the edges OA and OB of the body. Thus the leading edges will be in a region of expanding local flow with the fluid flowing around the edge of the body. Under these conditions, the aerodynamic heat transfer to the leading edges will be of the same order as that on the remainder of the lower surface and no special consideration would be required in this area. It will be noted that the sweep angle λ has no special significance as far as heat transfer is concerned for this case, since the basic heat transfer would be governed by the cone angle θ_c. This is in contrast to the Newtonian analysis which makes no allowance for cross flows and would therefore consider the swept edges OA and OB to be stagnation lines with no previous surface flow history. With this type of analysis, these edges would be subjected to high local heating and would require blunting to reduce the heat transfer along the entire leading edge.

With the assumption that the flow over a portion of a cone is to a first approximation identical to the flow over the entire cone, some useful properties of such a body can be investigated in terms of the cone angle θ_c and the meridion angle ϕ. For conical flow with the basic cone axis at zero angle of attack, the surface pressures are constant. The lift to drag ratio of the sharp conical configuration of Figure 1 can then be obtained as the ratio of surface area projected on a horizontal plane to that projected on a vertical plane normal to the flow. The horizontal projection of the surface area of a conical segment characterized by cone angle θ_c, meridion angle ϕ and base radius R (See Figure 1) is:

$$A_h = \frac{R^2 \sin \phi}{\tan \theta_c} \tag{1}$$

The surface area projected on a vertical plane is:

$$A_v = R^2 \phi \tag{2}$$

The lift to drag ratio becomes:

$$\frac{L}{D} = \frac{A_h}{A_v} = \left[\frac{1}{\tan \theta_c}\right]\left[\frac{\sin \phi}{\phi}\right] \tag{3}$$

The sweep back angle λ is given by:

$$\text{Tan}\,\lambda = \frac{\text{Sin}\,\phi}{\sqrt{\text{Cos}^2\,\phi + \frac{1}{\text{Tan}^2\,\theta_c}}} \qquad (4)$$

These properties are tabulated for various cone angles θ_c and meridion angles ϕ in the following tables.

Cone half angle

$\theta_c = 25°$

ϕ	L/D	λ
0°	2.145	0
15°	2.120	6.3°
25°	2.080	10.32°
35°	2.01	14.05°

$\theta_c = 35°$

ϕ	L/D	λ
0°	1.428	0
15°	1.410	8.55°
25°	1.383	14.07°
35°	1.340	19.25°

$\theta_c = 45°$

ϕ	L/D	λ
0°	1.00	0
15°	0.988	10.6°
25°	0.970	17.4°
35°	0.938	24.4°

$\theta_c = 55°$

ϕ	L/D	λ
0°	.700	0
15°	.691	12.25°
25°	.679	20.30°
35°	.656	28.05°

These tables show that L/D is a strong function of the design cone half angle θ_c and is much less dependent on meridion angle ϕ within the range shown. For $\phi = 90°$, $\frac{\text{Sin } \phi}{\phi} = 0.636$ so that for a half cone, the L/D is reduced substantially.

2.1.1 Conical Flow With Angle of Attack

The foregoing discussion covered the case of a conical body of the configuration shown in Figure 1, when this body is operated at an angle of attack α equal to the basic cone half angle θ_c. The flow field generated when the body of Figure 1 is at angles of attack greater or less than θ_c is more complicated and does not lend itself to rational analysis. Some insight into this situation may, however, be obtained from theories and experimental data on complete cones whose axes are at an angle of attack with respect to the flow. In this case, the inviscid flow over the body is no longer purely radial and there are cross flow components ω at right angles to the radii from the cone apex. These cross flow components are proportional to Sin ϕ and are therefore small in the vicinity of $\phi = 0$ and $\phi = 180°$. This is born out by tests of cones at high angles of attack where it is found that the surface pressure is reasonably constant for meridion angles ϕ between 0 and 25°. Typical test data from reference 1 are reproduced as Figures 2 and 3, Page 8. These figures show that when the cone axis is aligned at an angle of attack α' of $\theta_c/2$ or less, the surface pressure along the conical generators corresponding to $\phi = 25°$ is between 94% and 96% of the pressure along the generator at $\phi = 0$. In this case the angle of attack of a cone segment of Figure 1 would be $\alpha = \theta_c + \alpha'$. The data shown for $\phi = 155°$ would correspond to $\phi = 25°$ on the lower surface of a conical segment such as Figure 1 when operated at an angle of attack α less than θ_c. Here it is also seen when α' is equal to $\theta_c/2$ or less, the surface pressure is practically constant over a meridion angle of 25°. Thus, it can be concluded from these tests on complete cones that the surface pressure over a conical segment within 25° of the vertical meridion plane is essentially constant for basic cone angles of attack α' equal to $\theta_c/2$ or less.

2.2 Aerodynamic Configuration

The discussions of Section 2.1 can not be construed to present a rigorous discussion of the flow about cone segments of the type shown in Figure 1, however, if they are assumed to represent a first approximation, some conclusions can be drawn. These are:

EXPERIMENTAL VALUES OF PRESSURE COEFFICIENT
15° CONE M=3.53

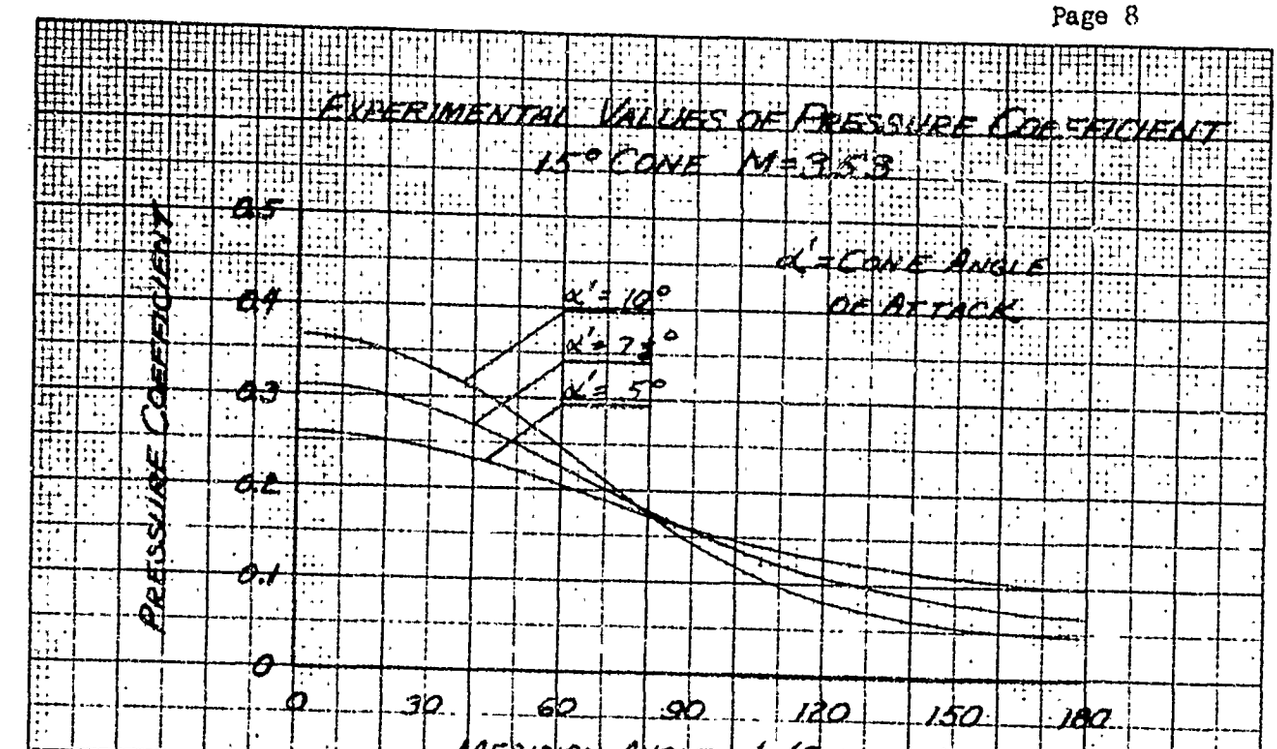

FIGURE 2

EXPERIMENTAL VALUES OF PRESSURE COEFFICIENT
20° CONE M=3.53

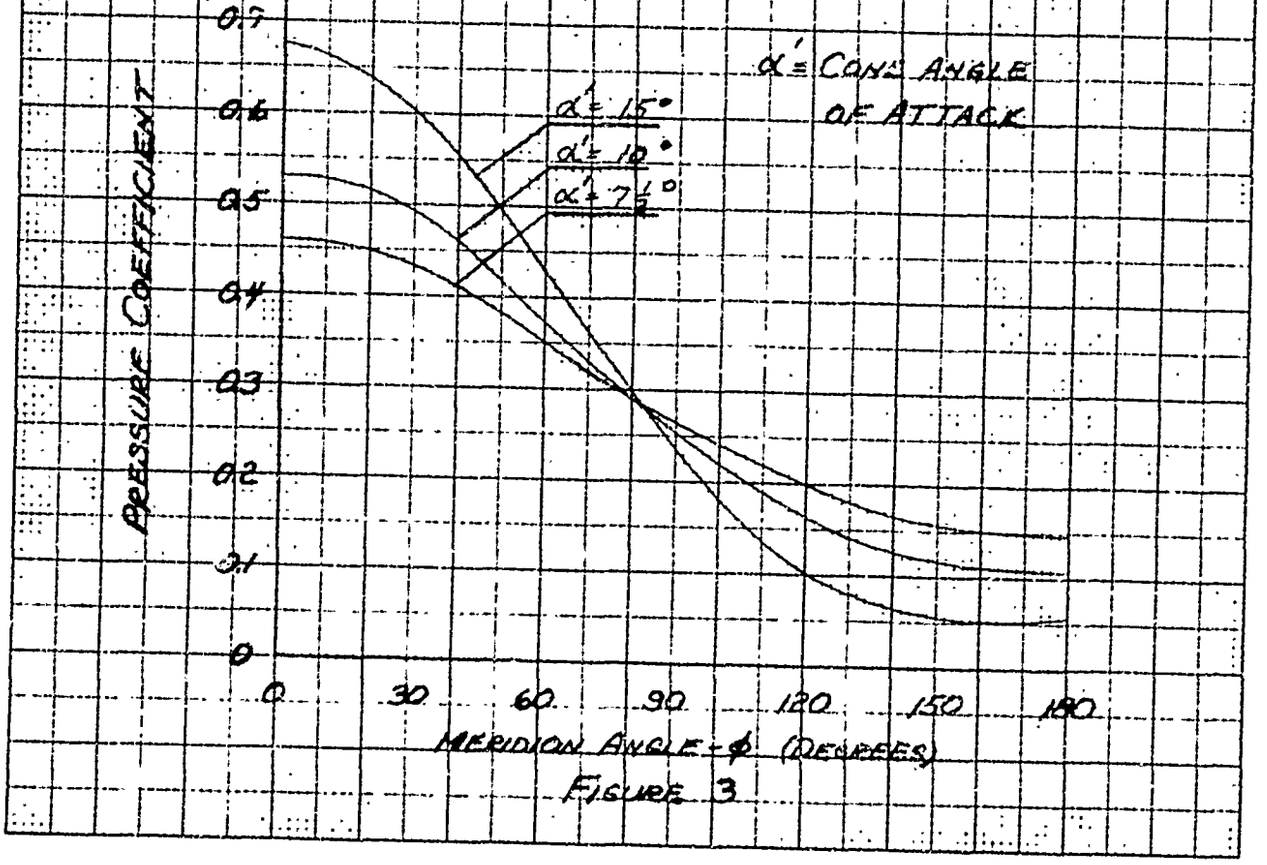

FIGURE 3

1. Meridion angle ϕ should be approximately 25° to maintain fairly uniform pressures over the lower lifting surface at all angles of attack.

2. The basic cone angle θ_c of Figure 1 should be approximately half way between the expected range of angle of attack.

For a vehicle angle of attack ranging from 15° to 55°, these conclusions give the following parameters:

$$\theta_c = 35°$$

$$\phi = 25°$$

For hypersonic flow (above M = 8) the stream is not able to flow around the lee side of the body and so the upper surface is of little consequence. For this case, it will be considered to be a modified half cone which is faired into the base. Three views of this configuration are shown in Figure 4, Page 10.

2.3 Vehicle Configuration

From previous data (reference 2) it has been found that a wing loading of 20 pounds per square foot is required to reduce surface temperatures to an acceptable level. It will further be assumed that an overall vehicle weight of 3000 pounds will be considered in the remainder of the investigation. These data, together with the aerodynamic configuration data yield the following vehicle characteristics:

$$\theta_c = 35°$$

$$\phi = 25°$$

$$\text{Wing area} = \frac{3000}{20} = 150 \text{ sq. ft.}$$

$$\text{Base radius } R = \sqrt{\frac{A}{\sin\phi\sqrt{\cos^2\phi + \frac{1}{\tan^2\theta_c}}}} = 14.5 \text{ ft.}$$

FIGURE 4

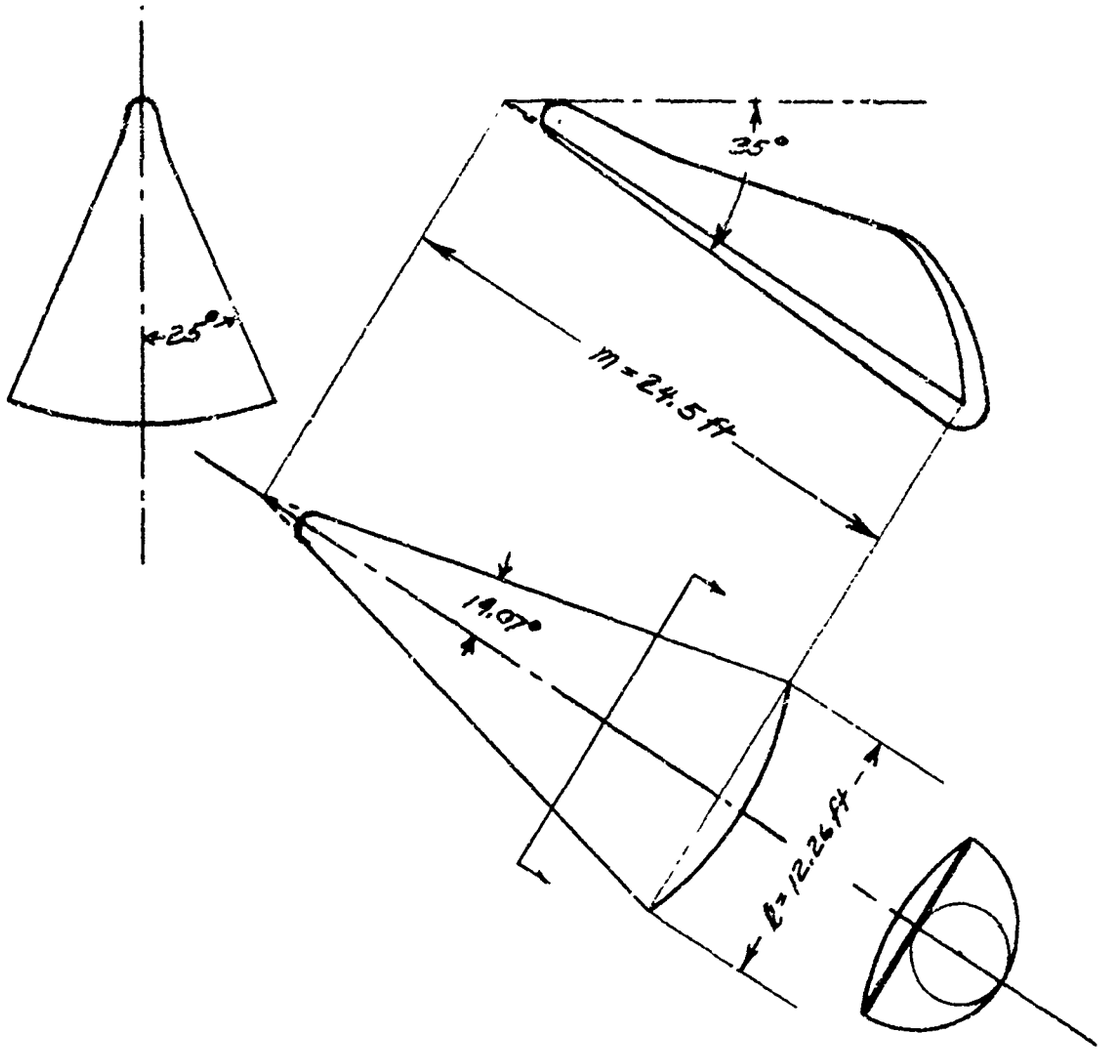

FIGURE 4

HYPERSONIC RE-ENTRY GLIDER
CONFIGURATION & DIMENSIONS

Length $N = R \sqrt{\cos^2 \phi + \frac{1}{\tan^2 \theta_c}} = 24.5$ ft.

Span $\ell = 2 R \sin \phi = 12.26$ ft.

Sweep angle $\lambda = 14.07°$

Normal radius at base $r = \frac{R}{\cos \theta_c} = 17.7$ ft.

The configuration and dimensions are shown on Figure 4.

2.4 Aerodynamic Heating

Previous analyses (reference 3) have shown that the maximum heating and therefore the maximum temperature will occur at a flight speed of 80% of orbital velocity. Since this is the maximum, the heat transfer and temperature distribution were estimated only for this condition.

The nose blunting requirements are estimated to limit the maximum stagnation temperature to 2500°F when operating at an angle of attack of 55°. They assumed the body to be equivalent to a cone having a half angle θ_c of 55° and resulted in a nose radius of 0.77 feet. The resulting temperature distribution over the lower surface of the body is shown in Figure 5. Details of these calculations are presented in Appendix A.

Figure 5 shows that temperatures above 2400°F occur over less than six inches of the body and temperatures over 2000°F are limited to the first foot. The greatest proportion of the body is at a temperature less than 1500°F. The nose temperature can be further reduced by increasing its radius with corresponding increases in vehicle drag. At lower angles of attack, the nose temperature will be proportionately higher than the body surface temperature because the nose pressures would be proportionately higher than the body surface pressures. However, this does not preclude flying at lower angles of attack and higher lift to drag ratio since at flight velocities removed from the velocity for maximum heating, the increased percentage of nose heating can be tolerated.

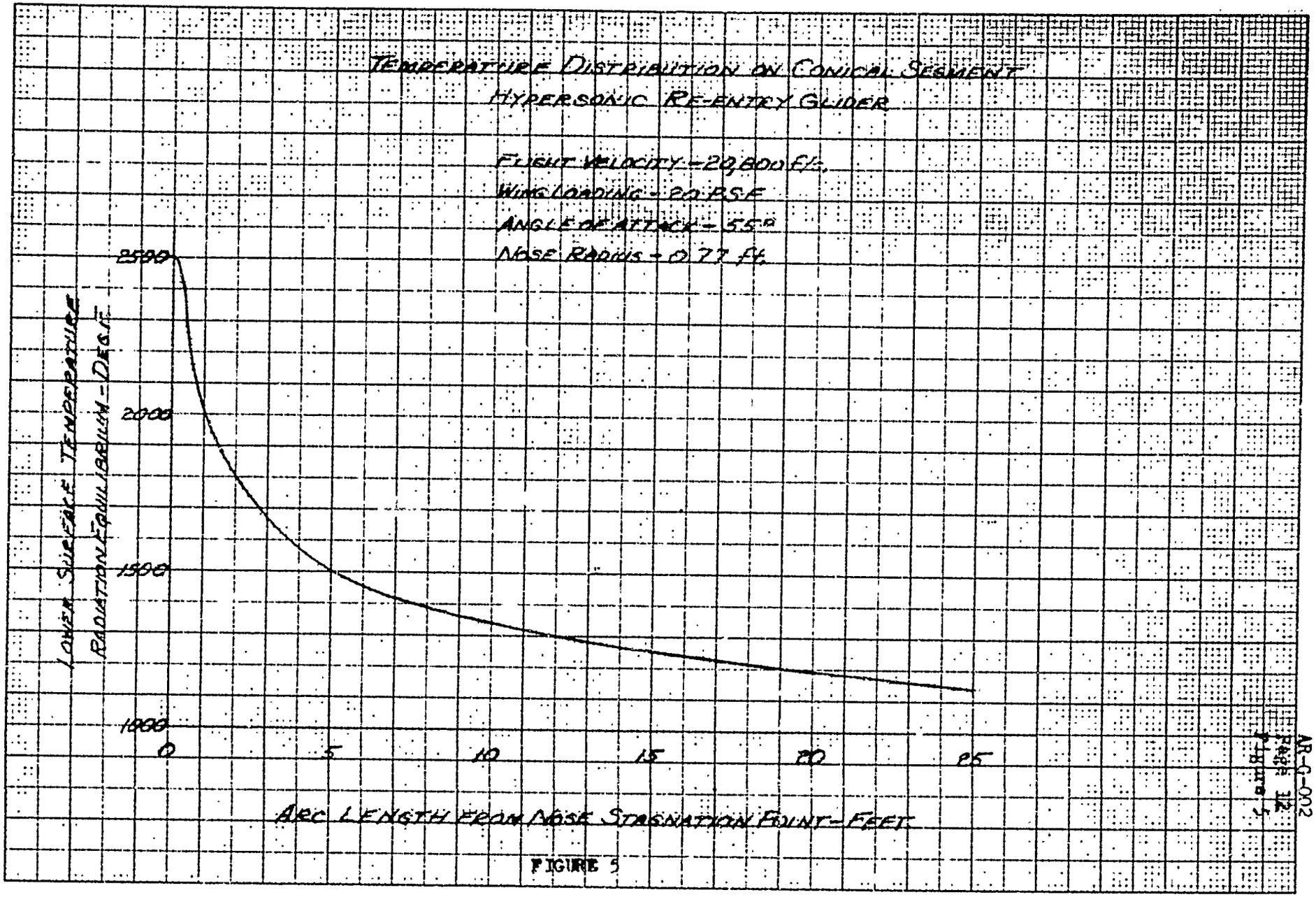
TEMPERATURE DISTRIBUTION ON CONICAL SEGMENT
HYPERSONIC RE-ENTRY GLIDER
FLIGHT VELOCITY = 20,800 F/S.
WING LOADING = 20 PSF
ANGLE OF ATTACK = 55°
NOSE RADIUS = 0.77 FT.
LOWER SURFACE TEMPERATURE
RADIATION EQUILIBRIUM - DEG. F
2500
2000
1500
1000
0
5
10
15
20
25
ARC LENGTH FROM NOSE STAGNATION POINT - FEET
AR-C-002

FIGURE 5

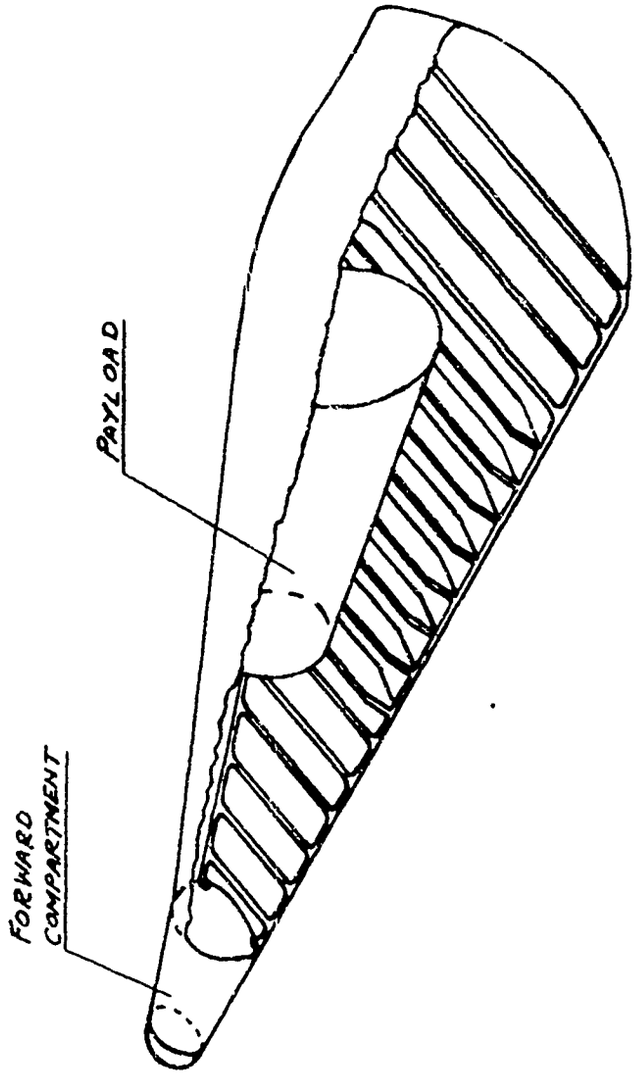

PRESSURIZED HYPERSONIC RE-ENTRY GLIDER
STRUCTURAL CONFIGURATION
FIGURE 6

3.0 Structural Design

The structure proposed for the vehicle shown in Figure 4 consists of a membrane type body pressurized to a pressure somewhat above the expected body surface pressures. The forward nose section is compartmented and pressurized to a higher pressure to sustain the pressure gradient in this area. A triangular framework supported by internal columns and beam columns reacts the collapsing load of the outer pressurized membranes. The payload which is assumed to be separate from the structure described above is supported by beams spanning the triangular framework. This structural arrangement is shown in Figure 6, Page 13.

3.1 Structural Loads

3.1.1 Pressure Loads

The maximum lower surface pressure during steady glide at hypersonic velocity will approach the basic wing loading as the relief due to flight centrifugal force decreases. The structure is also designed to sustain transient load factors or lift accelerations of 3.0. Under these conditions, the maximum surface pressure is

$$P_{s_{max}} = 3 \times 20 = 60 \text{ psf.}$$

In order to provide a suitable margin of excess pressure, an internal pressure of 120 psf gage is used on the marjority of the body.

The forward compartmented section may encounter external pressures as high as 900 psf. For this case, the internal pressure was assumed to be 1100 psf gage. These gage pressures are assumed to be referenced to the static pressure on the lower surface of the wing. This then leads to the following burst pressures:

Nose section
1100 psf (occurs at large angle of attack)
Body section
120 psf

The action of the internal pressure will lead to compressive loads in the struts which is proportional to the distance aft from the nose (actually the apex of the basic sharp cone). This load is distributed along the two leading edges and its magnitude is shown in Figure 7. It will be seen that the load varies linearly up to 164 pounds per inch of leading edge at the rear of the vehicle.

4.1.2 Inertia loads

For the present analysis, the payload capsule is assumed to weigh 2500 pounds with this load concentrated at the mid points of its supporting beams. Applying the transient load factor of 3.0, the beams must be designed to support a load of 7500 pounds distribution over them. The loads used in the analysis are shown in Figure 7.

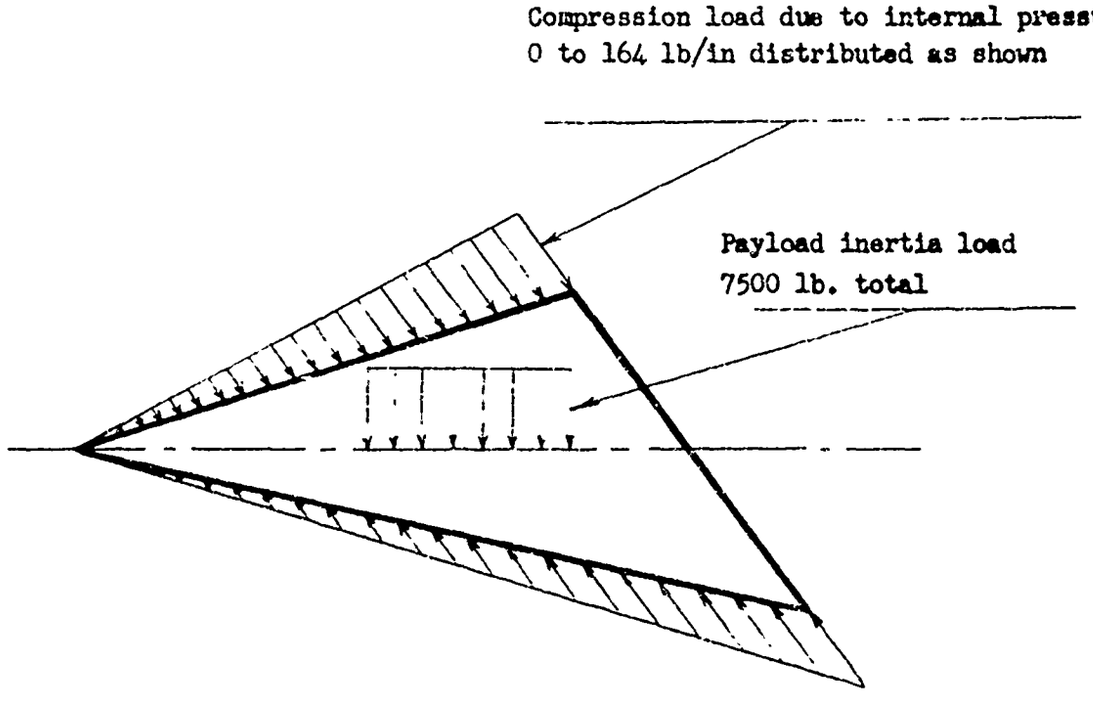

MAJOR LOADS USED IN RE-ENTRY GLIDER
STRUCTURAL ANALYSIS

FIGURE 7

3.2 Structural Weights

The characteristics of the various structural components are estimated in Appendix B. The summary of these in terms of structural weights is presented below.

Component	Dimensions	Material	Weight
Leading edge triangular frame	2.0" in Diam 0.040" in wall 46 feet long	steel	41.6 lb.
Beams to support payload	2.5" x 6.0" .030" side panels .050" cap strips	aluminum	69.1 lb.
Columns Forward of Payload	1.5" Diam. 0.040" wall 15 feet total	aluminum	3.4 lb.
Columns aft of payload	4.0" Diam. .028" wall 55' - total length	aluminum	23.1 lb.
Nose cap, Cone & fwd. bulkhead	Cone-,88 ft. base radius, .77 ft. fwd. radius, 2.28 ft. long, spherical end closures-.015" thick	columbium	13.0 lb.
Lower skin	Sector of circle 24' radius - 29° arc - 0.010 in. thick	columbium	69.0 lb.
Upper skin	Sector of circle 24' radius - 45° arc - 0.008 in thick.	columbium	86.6 lb.
Total Structural Weight			305.8 lb.

3.3 Pressurization Weight

While no detailed analysis of the pressurization system requirements was made, the gas required to fill the vehicle at sea level pressure was calculated as well as the weight of a pressure vessel required to contain the gas. The results are:

Weight of air	37.4 lb.
or	
Weight of helium	5.2 lb.
Storage bottle weight (titanium)	44.0 lb.

Total weight of bottle and gas:

Air	81.4 lb.
Helium	49.2 lb.

From the foregoing figures, the total of the major weight components is as follows:

Total Weight	
Air pressurization	387.2 lb.
Helium pressurization	355.0 lb.

4.0 Conclusions

The preliminary analysis presented in sections 2.0 and 3.0 indicate that a glide vehicle of the type shown in Figure 4 can provide a payload of approximately 2500 lbs. for a gross weight of 3000 lbs. This vehicle has a wing loading of 20 pounds per square foot and a maximum temperature of 2500°F at the stagnation point. The temperature over the greater portion of the body is less than 1500°F.

The major objective of this report is to establish design feasibility rather than to present complete design details. For this reason, many important design aspects such as aerodynamic trim and aerodynamic control have been omitted. In addition, careful thermal analyses of the temperature distribution in the internal structure may eliminate the use of aluminum.

In order to offset these omissions, simple and readily analysed internal structures were employed and the members were conservatively analysed. It is believed that more efficient structures can be designed within the above noted weights even when more accurate internal temperatures are used.

APPENDIX A

Aerothermodynamic Design Details

1.0 Nose Blunting

The nose blunting and body temperature distribution were estimated for the condition of maximum heating which occurs at 0.8 orbital velocity. The lift due to aerodynamic force results from a constant pressure acting on the lower surface (conical flow assumption). The body is oriented at an angle of attack of 55° and for the established wing loading, the surface pressure required to support the body may be calculated as follows:

$$P_W A \cos \alpha = W \left[1 - \left(\frac{u}{u_{orb}} \right)^2 \right] \qquad (A1)$$

where

P_W = Wing pressure - psf

A = Wing area - sq. ft.

α = Angle of attack

W = Vehicle weight

u = Flight velocity ft/sec

u_{orb} = Orbital velocity ft/sec

Solving for P_W, inserting the appropriate quantities and noting that $\frac{W}{A}$ = 20 psf,

P_W = 12.5 psf

If the pressure at the nose stagnation point is P_1 then the pressure at any other location away from the nose is given by (see sketch)

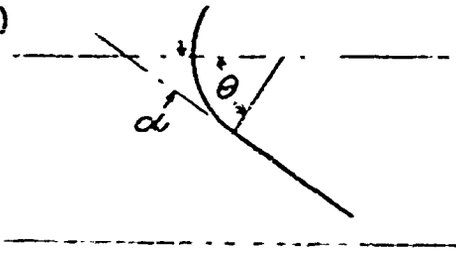

$$\frac{P}{P_1} = \text{Cos}^2\,\theta + \frac{1}{\gamma M_\infty^2}\,\text{Sin}^2\,\theta \qquad \text{(A2)}$$

Since P_W corresponds to the value of equation (A2) when $\theta = (90° - \alpha)$

$$\frac{P_W}{P_1} = \text{Cos}^2\,(90° - 55°) + \frac{1}{\gamma M_\infty^2}\,\text{Sin}^2\,(90° - 55°) = 0.671$$

and the nose stagnation pressure is

$$P_1 = \frac{P_W}{.671} = \frac{12.5}{.671} = 18.7 \text{ psf}$$

M. Romig in reference 4 gives the following expression for stagnation point heat transfer

$$q = 0.0145\, M_\infty^{3.1} \sqrt{\frac{P_\infty}{R_N}} \qquad \text{(A3)}$$

where

q = Heat transfer - Btu/ft^2/sec

M_∞ = Flight Mach number

P_∞ = Ambient pressure before nose shock wave pounds per square foot abs.

R_N = Nose radius - feet

But

$$\frac{P_1}{P_\infty} = \frac{1 + \gamma M_\infty^2}{1 + \gamma M_1^2} \sim 1 + \gamma M_\infty^2 \sim \gamma M_\infty^2 \qquad \text{(A4)}$$

where M_1 the Mach number after the shock is small so that γM_1^2 can be neglected.

Solving equation (A4) for P_{α} and substituting in equation (A3) gives

$$q = 0.0145\, M_{\alpha}^{2.1} \sqrt{\frac{P_1}{\gamma R_N}} \qquad (A5)$$

The heat transfer rate q which can be accepted by the nose is governed by the maximum allowable temperature for re-radiation. On the assumption that this can have a maximum value of 2500°F, q is 36.7 Btu/ft^2/sec and using this value in equation (A5) the value of R_N can be determined for the known flight condition. That is for P_1 = 18.7 psfa M_{α} = 21 2,

$$R_N = 0.77 \text{ ft.}$$

2.0 Body Surface Temperatures

The temperature distribution over the remainder of the body was calculated assuming the configuration to be similar to a blunt cone with a half cone angle of 55°. The methods used are outlined by Lees in reference 5.

3.0 Optimum Angle of Attack at Maximum Heating

While the angle of attack α of 55° was chosen somewhat arbitrarily to minimize the difference between the stagnation pressure P_1 and the body surface pressure P_W, the absolute value of P_1 is in fact the governing parameter (equation A5). For a given wing loading, W/A an expression for P_1 in terms of W/A and α can be obtained by solving equation A2 for P_W and substituting in equation (A1)

$$P_W = \frac{W}{A} \left[1 - \left(\frac{u}{u_{orb}} \right)^2 \right] \frac{1}{\cos \alpha} \qquad (A6)$$

$$\frac{P_W}{P_1} = \cos^2 (90 - \alpha) = \sin^2 \alpha \qquad (A7)$$

Solving equation (A7) for P_W, substituting in equation (A6) and solving for nose stagnation pressure P_1 gives

$$P_1 = \frac{W}{A}\left[1 - \left(\frac{u}{u_{orb}}\right)^2\right] \frac{1}{\sin^2\alpha \cos\alpha} \qquad (A8)$$

For P_1 to be a minimum, $\sin^2\alpha \cos\alpha$ should be a maximum. Differentiating and setting the result equal to zero

$$\sin\alpha\left[2\cos^2\alpha - \sin^2\alpha\right] = 0$$

$$\frac{\sin^2\alpha}{\cos^2\alpha} = \tan^2\alpha = 2$$

$$\alpha = 54.8^\circ$$

4.0 Blunt Body Lift to Drag Ratio

The lift to drag ratios given in section 2.1 are for sharp conical segments. The addition of the blunt spherical cap adds an approximately constant pressure drag to the drag force described in section 2.1 (ie the projected area on a vertical plane normal to flight direction). This additional drag was estimated by integrating the Newtonian pressure forces on the nose and adding these to the body surface pressure forces acting in the drag direction. The results are tabulated below.

α	L/D Blunt Body
15	2.707
25	1.930
35	1.344
45	0.955
55	0.672

APPENDIX B

Structural Design Details

The basic structure is described in section 3.0 and Figure 6. The applied loads are discussed in paragraph 3.1 and shown in Figure 7. Utilizing this information, limited estimates were made of the size of structural elements required to carry these loads. In general, conservative estimates were made to allow for items which a more detailed investigation might uncover. The analysis of the principal structural elements is presented below.

1.0 Leading Edge Support

The leading edges act as a beam with a distributed load increasing uniformly to the maximum value of 164 pounds per inch. This distributed load is reacted periodically by the compression struts supporting the two leading edge beams. The leading edge beams are circular in cross section and because of the high temperature were assumed to be steel with an allowable stress σ of 20,000 psi. These leading edges will have the same temperature distribution as the lower surface shown in Figure 5 and start about 3.0 ft. from the stagnation point. Since the leading edges are continuous over many supports, a single span was approximated by the relations for a fixed ended beam. In this case, the maximum bending moment is

$$M = \frac{q\, l^2}{12}$$

where

M = bending moment - in-lbs.

q = load - pounds per inch

l = span between supports

Preliminary calculations indicate that a tube of 1.0 in radius and 0.040 in wall thickness will lead to a low weight structure. For these dimensions, the allowable span between struts is given by

$$l^2 = 3\pi \left[r^2 - (r - \Delta r)^2 \right] \frac{\sigma}{r\, q}$$

$$l = 14.25 \text{ inches}$$

when the distributed load q is 140 pounds per inch. The actual span between beam columns was taken to be 10.7 inches for purposes of strut and beam design so that the stress would be less than 20,000 psi. in the leading edge beam. The leading edges are each 23 ft. long and, with the dimensions selected, their weight is

$$Wt = (2)\ (23)\ (2\pi)\ (1)\ (.040)\ (.3)\ (12) = 41.6 \text{ pounds.}$$

2.0 Payload Supporting Beam Columns.

The payload will constitute most of the weight of the vehicle and should therefore be located in the vicinity of the center of pressure. The center of pressure acts about 2/3 of the distance aft from the nose and for this analysis, the payload was assumed to extend over a distance of 8.0 ft. starting 11.0 ft. aft from the nose. This payload is supported by beam columns 10.7 inches on center which also support the leading edge beams described above. As the beams are 10.7" apart over an 8 ft. interval, there are

$$\frac{96}{10.67} = 9 \text{ Beams}$$

The maximum load supported by all beams is the payload (2500 lb) times the load factor (3) so the load on an individual beam is

$$\frac{2500 \times 3}{9} = 835 \text{ lb.}$$

Only the beam of maximum span was analysed. This is an aluminum beam with a span of 10 ft. Since the payload was assumed to act at the center, the maximum beam bending moment is

$$M = \frac{P}{2} \times \frac{1}{2} = \frac{835}{2} \times \frac{10 \times 12}{2} = 25{,}000 \text{ in. lb.}$$

At the station where this beam is located, the compressive load is 140 pounds per inch so the column load is

$$P = 140 \times 10.67 = 1492 \text{ pounds}$$

A number of configurations were analysed but only the final version is described below

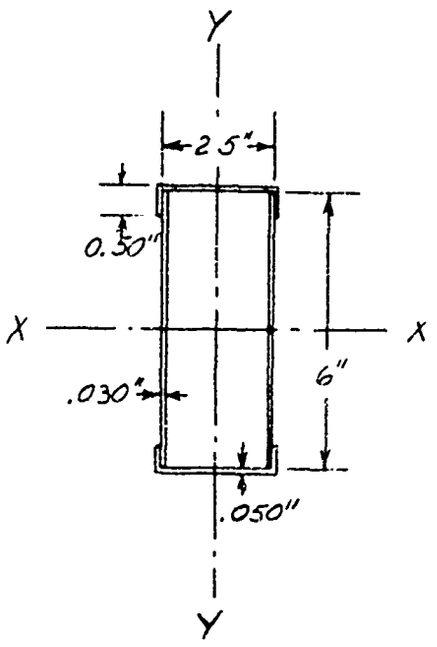

$$I_{xx} = 2 \times (2.5 \times .050 \times 3.0^2) + \frac{1}{12} 2(.030)(6^2)$$

$$I_{xx} = 2.43 \text{ in}^4$$

$$I_{yy} = 2(6 \times .030 \times (1.25)^2) + \frac{1}{12} (2)(.050)(2.5)^3$$

$$I_{yy} = 0.692 \text{ in}^4$$

Note: The 1/2 inch flanges on the top and bottom caps are neglected for both I_{xx} and I_{yy}.

Bending stress in beam at extreme fibers

$$\sigma = \frac{Mc}{I_{xx}} = \frac{(25{,}000)(3.0)}{2.43} = 30{,}900 \text{ psi.}$$

Shear stress on neutral axis

$$T = \frac{V\,Q}{t I_{xx}}$$

where

V = shear

Q = $\int$ yda

t = thickness

$$Q = 2 \times (.030)(3.0)(1.5) + 2.5 \times (.050)(3)$$

$$= 0.645 \text{ in}^3$$

$$V = \frac{835}{2} = 417.5 \text{ lb.}$$

$$\tau = \frac{(417.5)(.645)}{(.060)(2.43)} = 1850 \text{ psi}$$

The critical shear stress for stiffened panels is given by

$$\tau_{s\ crit} = K \frac{\pi^2 E t^2}{12(1-\mu^2)\ b^2}$$

where

E = Young's modulus = 10^7 for aluminum

t = Thickness of panel

b = Stiffener spacing - see sketch

μ = Poisson's ratio

K = Constant depending on stiffener spacing - function of a/b

a = Beam depth.

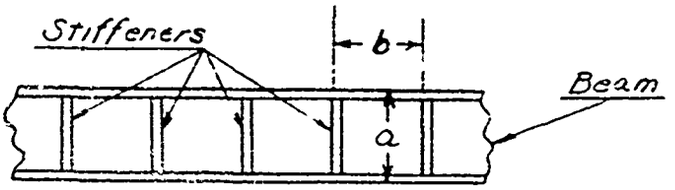

For a = b = 6.0 in, K = 9.4 and

$$\tau_{s_{crit}} = 9.4 \times \frac{9,87 \times 10^7\ (,030)^2}{12\ (1-.3^2)\ (36)} = 2120 \text{ psi}$$

which exceeds the applied shear stress of 1850 psi. Strength of the beam as a column.

$$P_c = \frac{\pi^2 E I_{xx}}{l^2} = \frac{(9,87 \times 10^2)(2,43)}{(120)^2} = 16,700 \text{ lb.}$$

Since this is large compared to the applied column load, beam column is satisfactory.

Column load about y-y axis is given by

$$P_c = \frac{\pi^2 E I_{yy}}{l^2} = 4720 \text{ lb. which is nearly three times the applied load of 1500 lb.}$$

Although the stiffeners need only be located at 6 inch intervals, beam weight estimates were based upon 4 in. spacing. With the foregoing dimensions, the weight per foot of the beam is

$$\text{wt/ft} = \left[12\left\{\left[3.5 \times .050 \times 2\right]+\left[6 \times .030 \times 2\right]\right\}+(1 \times .030 \times 6)(3)(2)\right] 0.1$$
$$= 0.96 \text{ lb/ft.}$$

Although the remainder of the beams are shorter and have a lower column load, they were assumed to have the same weight per foot as the beam analysed above. The nine beams have a minimum length of 6 ft. and a maximum length of 10 ft. for an average of 8 feet. With the weight per foot above, the total beam weight is

$$\text{wt} = 9 \times 8 \times 0.96 = 69.1 \text{ lb.}$$

The selection of aluminum for this application may not be feasible unless radiation heat transfer can be limited by a very low emissivity finish on the inner surfaces. In any event, titanium would be satisfactory but might introduce weight increases in the beams of 50%. It would also be possible to use a truss structure surrounding the payload which should reduce the supporting structural weight. Time did not permit analysis of this more complicated structure.

3.0 Compression struts

In addition to the beam columns of section 2.0 there are pure compression columns forward and aft of the payload. These were estimated using long column critical buckling criteria. Forward of the payload, the compressive load varies from 0 to 55 lb/inch of leading edge and the columns vary from 0 to 5 ft. in length. Forward of the payload, the span of the leading edge beams can be increased to 20.0 inches because of the reduced compressive load resulting from the smaller radius of curvature of the lower skin. For this span, the stress in the leading edge beam is

$$\sigma = 15{,}500 \text{ psi}$$

when the distributed load is 55 lbs. per inch. The longest column has a load of 1100 lbs. (55 lbs. per in. times 20 inch span). For this case a circular aluminum column having the following dimensions was satisfactory

D = 1.5 inches

t = 0.040 inches

$$I = \frac{\pi}{4}\left[(.75)^4 - (.71)^4\right] = 0.0596$$

$$P_c = \frac{\pi^2 E I}{\ell^2} = \frac{(9.87)(10^7)(.0596)}{(60)^2} = 1316 \text{ pounds}$$

The distance to the nose is 9 ft. and with columns at 20 inch intervals, there are 5 1/2 or 6 columns with an average length of 2.5 ft.

$$wt = \pi(1.5)(.040)(30)(.10)(6) = 3.4 \text{ lb.}$$

Columns may not be required in the forward closed compartment but they were included for weight purposes.

Aft of the payload, there is a distance of 4 ft. to the rear of the vehicle where columns are required to support the leading edge beams. Here the compressive load goes up to 164 pounds per inch. The columns were taken 10 inches on centers so that five of them are required. While the maximum load is 1640 lb., the longest column (12 ft) was designed to support a load of 3000 lb. and columns of the same cross section were used at the other locations. An aluminum column with 4.0 in diameter and 0.028 wall thickness was selected for this case

$$I = \frac{\pi}{4}\left[(2.0)^4 - (1.972)^4\right] = 0.63 \text{ in.}^4$$

$$P_{cr} = \frac{\pi^2 E I}{\ell^2} = \frac{(9.87)(10^7)(.63)}{(144)^2} = 3{,}000 \text{ lb.}$$

There are five columns with an average length of 11.0 ft. The resulting weight is

$$wt = 5 \times (11 \times 12)(2\pi)(2.0)(.028)(.1) = 23.1 \text{ lb.}$$

4.0 Nose Compartment

The forward nose compartment is a truncated cone with hemispherical end closures and has the dimensions shown below.

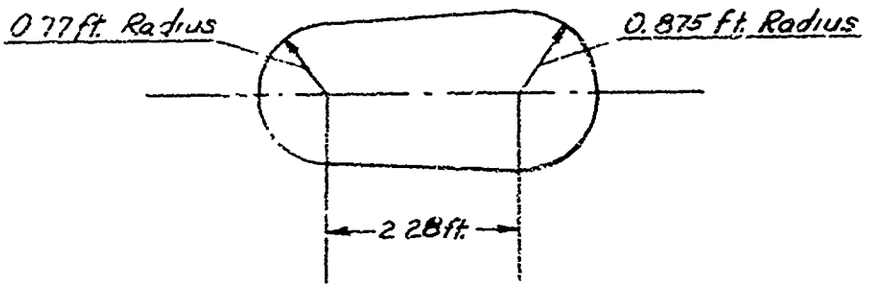

From section 3.1.1, the internal pressure exceeds the external pressure by 1100 psf. For the spherical cap at a temperature of 2500°F, the allowable stress is σ = 2340 psi.

Cap thickness is then

$$t = \frac{Pr}{2\sigma} = \frac{1100}{144} \times \frac{(.77)(12)}{2(2340)} = 0.015 \text{ in.}$$

For the conical section following the cap, the temperature is down to 2000°F with an allowable stress σ of 11,700 psi. At the rear of this section, the minimum thickness is

$$t = \frac{Pr}{\sigma} = \frac{1100}{144} \times \frac{(.875)(12)}{11,700} = 0.00705 \text{ in.}$$

The weights were estimated on the basis of a constant thickness of 0.015 in. for cap, conical section and rear closure. The total weight is 13.02 lb.

5.0 Lower Skin or Membrane

The lower skin starts 3 ft. from the nose and extends to 24 ft. from the nose. Because the temperature and radius of curvature vary over this distance, the skin was divided into sections. The temperature used was that at the beginning of the section and the radius of curvature was that at the end of each section. The thickness was obtained from

$$t = \frac{Pr}{\sigma}$$

where

P = Internal pressure = 120 psf (.833 psi) from section 3.1.1

r = s tan 35° where s is distance from nose to end of section in question.

σ = Allowable stress.

The results are tabulated below

Section	Temperature	Stress	Thickness	Thickness used
3' to 5'	1670°F	16,100 psi	.0029 in.	.010 in.
5' to 9'	1500°F	20,000 psi	.0037 in.	.010 in.
9' to 12'	1370°F	20,000 psi	.0048 in.	.010 in.
12' to 16'	1300°F	30,000 psi	.0041 in.	.010 in.
16' to 20'	1240°F	30,000 psi	.0051 in.	.010 in.
20' to 24'	1190°F	30,000 psi	.0060 in.	.010 in.

A minimum gage of 0.010 in. was used at all stations to give the following weight.

Wt = 69.0 lb.

6.0 Upper Skin or Membrane

The upper membrane is a half cone except near the rear of the vehicle. Because of its much smaller radius of curvature, the stresses are quite low and it was assumed that a minimum gage of 0.008 inches could be used. For ease of calculating it was assumed that the actual area would be approximated by a cone that went all the way to the rear with no end closure. For this shape and thickness, the weight is as follows:

Wt = 86.6 lbs.

7.0 Pressurizing Gas and Gas Storage Bottle

The internal volume of the vehicle was taken equal to that of a half cone extending to the end of the vehicle. This volume is 459 cu. ft. and requires 37.4 pounds of air or 5.0 pounds of helium to maintain the 16 psi absolute required to pressurize the vehicle at sea level. Since the initial internal pressures are very small, this gas must be stored aboard the vehicle. A sphere 21.24 in. in diameter is required to contain either gas at a pressure of 2500 psi using titanium with a stress level of 70,000 psi, this requires a wall thickness of 0.19 in. and the bottle weighs 44 lb.

REFERENCES

1. Holt, Maurice and Blackie, John, "Experiments on Circular Cones at Yaw in Supersonic Flow", Journal of the Aeronautical Sciences, Vol. 23, No. 10, P. 931, October 1956.

2. Hanley, G. M., "Aerodynamic Heating on a Flat Plate During Hypersonic, Quasi-Steady, Gliding Flight". Convair-Astronautics Report AZJ-001 T.N., June 20, 1958.

3. Hanley, G. M., "Hypersonic Stagnation Region Heating", Convair-Astronautics Report AZJ-002 T.N., October 8, 1958.

4. Romig, M. F., "Stagnation Point Heat Transfer for Hypersonic Flow", Jet Propulsion, Vol. 26, December 1956, pp. 1098-1099.

5. Lees, Lester, "Laminar Heat Transfer Over Blunt-Nosed Bodies at Hypersonic Flight Speeds", Jet Propulsion, Vol. 26, April 1956, pp. 259-269.